Author Manuscript

Author Manuscript

Author Manuscript

Author Manuscript

HHS Public Access

Author manuscript

SIAM J Appl Dyn Syst. Author manuscript; available in PMC 2017 September 19.

Published in final edited form as:

SIAM J Appl Dyn Syst. 2016 ; 15(4): 1844–1873. doi:10.1137/15M1031965.

Stability of Systems with Stochastic Delays and Applications to Genetic Regulatory Networks

Marcella M. Gomez[*], **Mehdi Sadeghpour**[†], **Matthew R. Bennett**[‡], **Gábor Orosz**[†], and **Richard M. Murray**[§]

[*]Electrical Engineering and Computer Science, University of California, Berkeley, CA 94720, USA

[†]Department of Mechanical Engineering, University of Michigan, Ann Arbor, MI 48109, USA

[‡]Department of BioSciences and Department of Bioengineering, Rice University, Houston, TX 77005, USA

[§]Control and Dynamical Systems, California Institute of Technology, Pasadena, CA 91125, USA

Abstract

The dynamics of systems with stochastically varying time delays are investigated in this paper. It is shown that the mean dynamics can be used to derive necessary conditions for the stability of equilibria of the stochastic system. Moreover, the second moment dynamics can be used to derive sufficient conditions for almost sure stability of equilibria. The results are summarized using stability charts that are obtained via semi-discretization. The theoretical methods are applied to simple gene regulatory networks where it is demonstrated that stochasticity in the delay can improve the stability of steady protein production.

Keywords

stability; stochastic delay; systems biology; genetic networks

1. Introduction

Time delays are a well known source of instability in dynamical systems and can make control design a challenging task. When the delays are assumed to be constant or distributed, there are well established methods to analyze stability and bifurcations of equilibria and periodic orbits [7, 9, 19, 24, 45, 46]. When the delays depend on time or on the state of the system, stability analysis becomes more difficult and may require averaging or numerical techniques [18, 20, 37]. However, in some cases delays vary stochastically in time, making it very challenging to characterize stability. In this paper, we target the problem of stability analysis of systems with stochastically changing delays. Stochastic delays arise in networked control systems [5], connected vehicles [43], and gene regulatory networks [15, 21].

When investigating dynamics under stochastic delay variations, key factors include the stochastic process describing the time evolution of the delay and the type of stability investigated. In early works, random delays modeled by continuous-time Markov chains were incorporated into delay differential equations [22, 29] and Lyapunov stability theorems were used to obtain sufficient conditions of stability. This approach has been extended to

Author Manuscript Author Manuscript Author Manuscript Author Manuscript

nonlinear systems [25] and has also been applied to discrete-time systems where the corresponding matrix inequalities again give sufficient stability conditions [12, 41, 55]. These conditions are typically quite conservative, which makes it difficult to evaluate the effect of the delays on the dynamics. Similarly, taking the worst case scenario (e.g., largest delay) can lead to unnecessary conservativeness or may simply give erroneous results. Even ensuring stability for each value of the delay does not necessarily give the stability of the stochastic system [13].

Work has also been done comparing stability conditions for different types of stability (Lyapunov stability, moment stability, almost sure stability) for a continuous-time linear system under specific delay variations [51]. In this paper we expand these ideas to a broader class of delay processes, while focusing on moment stability, almost sure stability, and the relationship between these. We use a technique called semi-discretization [19] to classify different stability losses and to derive stability charts.

To demonstrate the power of the developed mathematical tools, we apply them to simple gene regulatory networks where a protein represses its own production. Traditional mass-action kinetic models are based on instantaneous reactions and model the time evolution of protein concentrations by ordinary differential equations (ODEs), which can be used to characterize the dynamics about equilibria and periodic solutions [6]. However, the protein production process comprises of a sequence of biochemical reactions and, thus, a fully mature protein only becomes available after some time delay. Consequently, a more accurate way to describe the dynamics of genetic regulatory networks is to use delay differential equations (DDEs), which still allows one to investigate stability and bifurcations [28, 38]. For instance, it has been shown that delay may lead to oscillations in models with negative delayed feedback in synthetic gene networks [35, 47, 49].

The intracellular environment is inherently noisy [36] and stochasticity is often incorporated into modeling equations by simply adding Gaussian noise. Such studies have been extended to gene networks modeled with delays [48]. However, the biochemical processes that are lumped together by the delay are also stochastic in nature, which results in stochastic delay variations [15, 21]. We analyze corresponding effects and produce stability charts for equilibria on the plane of gain parameters for different distributions of the stochastic delay. The stability results are also validated using numerical simulations of the linearized and nonlinear models.

2. Continuous-time Systems with Stochastic Delay

In this paper we consider systems of the form

$$\dot{\chi}(t)=f(\chi(t),\chi(t-\tau(t))), \quad (2.1)$$

where dot denotes the derivative with respect to time t, $\chi \in \mathbb{R}^n$, $f\colon \mathbb{R}^n \times \mathbb{R}^n \to \mathbb{R}^n$, and the delay $\tau \in \mathbb{R}$ varies in time stochastically. More precisely we assume that the delay follows a stationary stochastic process with probability distribution $w(\sigma)$, $\sigma \in [\tau_{\min}, \tau_{\max}]$. Thus, the

Author Manuscript Author Manuscript Author Manuscript Author Manuscript

initial condition is given by $\chi(t) = \chi_0(t)$, $t \in [-\tau_{\max}, 0]$. Due to the stochasticity in the delay, the vector $\chi(t)$ also follows a stochastic process.

Linearizing equation (2.1) about an equilibrium $\chi(t) = \chi_*$ results in the system

$$\dot{x}(t)=\mathbf{a}x(t)+\mathbf{b}x(t-\tau(t)), \quad (2.2)$$

where $x(t) = \chi(t) - \chi_*$, $\mathbf{a} = \partial_1 f(\chi_*, \chi_*)$, $\mathbf{b} = \partial_2 f(\chi_*,\chi_*) \in \mathbb{R}^{n\times n}$, and ∂_1 and ∂_2 represent derivatives with respect to the first and second variables, respectively. In this paper, we analyze the equations describing the first and second moments of the linear system (2.2). Note that equations describing the first and second moments of the nonlinear system (2.1) may differ from these in a general case.

We consider a class of delay processes where the delay trajectories are piece-wise constant functions of time. Namely we assume that the delay $\tau(t)$ may only take J possible discrete values from the set $\{\tau_1, \tau_2, \ldots, \tau_J\}$ with $\mathbb{P}[\tau(t) = \tau_j] = w_j$, where $\mathbb{P}$ denotes probability. Without loss of generality we can consider $\tau_1 < \tau_2 < \cdots < \tau_J$. In this case, the corresponding probability density function (pdf) consists of Dirac deltas, that is,

$$w(\sigma)=\sum_{j=1}^{J} w_j \delta(\sigma-\tau_j), \quad (2.3)$$

where $\int_{\tau_{\min}}^{\tau_{\max}} w(\sigma)\mathrm{d}\sigma=\sum_{j=1}^{J} w_j=1$. From here on, we use the term pdf and delay distribution interchangeably. Note that one can approximate continuous delay distributions by increasing the density of the Dirac deltas. Also we assume that the delay stays constant for a holding time T before potentially taking on a new value, as demonstrated by the sample realization in Fig. 2.1 for $J = 3$ different delay values. Since the probability distribution in (2.3) is not changing with time, the delays assumed across the holding intervals are independent and identically distributed (IID). In this paper, we focus on stability analysis of systems in the form of (2.2) with stated assumptions on the delay, while linear approximations and numerical simulations are used to investigate nonlinear phenomena in nonlinear systems of type (2.1).

Taking the expected value, denoted by $\mathbb{E}$, of system (2.2) we obtain

$$\frac{\mathrm{d}}{\mathrm{d}t}[x(t)]=\mathbf{a}[x(t)]+\mathbf{b}\sum_{j=1}^{J}[\tau(t)=\tau_j][x(t-\tau_j)|\tau(t)=\tau_j]. \quad (2.4)$$

Author Manuscript Author Manuscript Author Manuscript Author Manuscript

If the holding time T is smaller than the minimum delay, i.e., $T < \tau_1$ then $x(t-\tau_j)$ is independent of $\tau(t)$ due to the IID nature of the delay sequence. Thus, introducing the notation $\bar{x} = \mathbb{E}[x]$, we obtain

$$\dot{\bar{x}}(t) = \mathbf{a}\bar{x}(t) + \mathbf{b}\sum_{j=1}^{J} w_j \bar{x}(t-\tau_j). \tag{2.5}$$

Generalizing this for any stationary stochastic delay process where the autocorrelation of the delay becomes zero after T and $T < \tau_{\min}$ yields the general form

$$\dot{\bar{x}}(t) = \mathbf{a}\bar{x}(t) + \mathbf{b}\int_{\tau_{\min}}^{\tau_{\max}} w(\sigma)\bar{x}(t-\sigma)\mathrm{d}\sigma. \tag{2.6}$$

The distributed delay systems (2.5) and (2.6) describe the dynamics of the mean and they can be analyzed using standard stability and bifurcation analysis tools [9, 45, 46]. The mean dynamics can provide some information about the effect of stochastic delays as they explicitly contain the delay distribution. However, to characterize the stochastic dynamics one needs to analyze higher moments.

In order to analyze the higher moments of the continuous-time system (2.2), we discretize it by dividing the holding intervals of length T into $\ell \in \mathbb{N}$ subintervals of length $\Delta t = T/\ell$, see Fig. 2.1. Then, using a time discretization technique, called semi-discretization [19], we construct a discrete-time map as a discretization of (2.2) which allows us to obtain conditions for the stability of the mean and the second moment. Then, we demonstrate the convergence of the corresponding spectra and stability charts when $\Delta t \to 0$.

To apply semi-discretization we assume that the delayed term in (2.2) stays constant in the time interval $t \in [i\Delta t, (i+1)\Delta t)$, that is,

$$\dot{\tilde{x}}(t) = \mathbf{a}\tilde{x}(t) + \mathbf{b}\tilde{x}(i\Delta t - r(i)\Delta t), t \in [i\Delta t, (i+1)\Delta t), \tag{2.7}$$

where $r(i) \in \mathbb{Z}^+$ takes the values $\{r_1, \ldots, r_J\}$ with $r_j = \left\lfloor \frac{\tau_j}{\Delta t} \right\rfloor$, $j = 1,\ldots, J$, for $i = 0,1,2,\ldots$ In other words, the delay values are rounded off by the mesh size Δt. Since equation (2.7) is a linear differential equation with constant forcing, it can be solved in the time interval $t \in [i\Delta t, (i+1)\Delta t)$ yielding

$$\tilde{x}(i+1) = \boldsymbol{\alpha}\tilde{x}(i) + \boldsymbol{\beta}\tilde{x}(i - r(i)), \tag{2.8}$$

where

Author Manuscript Author Manuscript Author Manuscript Author Manuscript

$$\boldsymbol{\alpha}=\mathrm{e}^{\mathbf{a}\Delta t},\boldsymbol{\beta}=\left(\int_0^{\Delta t}\mathrm{e}^{\mathbf{a}(\Delta t-t)}\mathrm{d}t\right)\mathbf{b}, \quad (2.9)$$

and we have used the notation $\tilde{x}(i) = \tilde{x}(i\Delta t)$. We remark that if $\mathbf{a}^{-1}$ exists, then the second formula results in $\boldsymbol{\beta} = (\mathrm{e}^{\mathbf{a}\Delta t} - \mathbf{I})\,\mathbf{a}^{-1}\mathbf{b}$, where $\mathbf{I}$ is the n-dimensional identity matrix.

Let us define the augmented vector $X(i) = [\tilde{x}^{\mathrm{T}}(i)\ \tilde{x}^{\mathrm{T}}(i-1)\cdots\tilde{x}^{\mathrm{T}}(i-r_J)]^{\mathrm{T}} \in \mathbb{R}^{(r_J+1)n}$, where T denotes the transpose. Then equation (2.8) can be written in the compact form

$$X(i+1)=\mathbf{G}(i)X(i), \quad (2.10)$$

where the matrix $\mathbf{G}(i)$ follows a stochastic process and takes the values

$$\mathbf{G}_j=\begin{bmatrix} \boldsymbol{\alpha} & \mathbf{0} & \cdots & \boldsymbol{\beta} & \cdots & \mathbf{0} \\ \mathbf{I} & \mathbf{0} & \mathbf{0} & \cdots & \mathbf{0} & \mathbf{0} \\ \mathbf{0} & \mathbf{I} & \mathbf{0} & \cdots & \mathbf{0} & \mathbf{0} \\ \mathbf{0} & \mathbf{0} & \mathbf{I} & \cdots & \mathbf{0} & \mathbf{0} \\ \vdots & \vdots & \vdots & \ddots & \vdots & \vdots \\ \mathbf{0} & \mathbf{0} & \mathbf{0} & \cdots & \mathbf{I} & \mathbf{0} \end{bmatrix} \in {}^{(r_J+1)n\times(r_J+1)n}, \quad (2.11)$$

with probability w_j for $j = 1,\ldots, J$.

The first block row in matrix $\mathbf{G}_j$ corresponds to the delay τ_j in (2.8) and therefore it changes when the delay changes such that the block $\boldsymbol{\beta}$ is in the $(r_j + 1)$-th block-column. Note that given that the delay holding time $T = \ell\Delta t$, the matrix $\mathbf{G}_j$ is kept constant for ℓ time steps before changing. Thus defining $Y(k) = X(k\ell)$, $k = 0,1,2,\ldots$ the system (2.10) can be written as

$$Y(k+1)=\mathbf{A}(k)Y(k), \quad (2.12)$$

where $\mathbf{A}(k)$ takes values

$$\mathbf{A}_j=(\mathbf{G}_j)^{\ell} \in {}^{(r_j+1)n\times(r_j+1)n}, \quad (2.13)$$

and $\mathbb{P}\ [\mathbf{A}(k) = \mathbf{A}_j]$ is w_j, $j = 1,\ldots, J$. Since the delays of different holding intervals are IID the matrices $\mathbf{A}(k)$ are IID and $\mathbf{A}(k)$ is independent of $Y(k)$.

Author Manuscript Author Manuscript Author Manuscript Author Manuscript

3. Stability Conditions

In this section, we establish conditions for stability of the stochastic dynamical system (2.12), that is the discretization of system (2.2). We focus on almost sure stability, which is obtained by calculating second moment stability. Let us start with some definitions.

Definition 3.1. A random sequence $\{X(k) \in {}^n\}_{k=0}^{+\infty}$ **converges to 0 almost surely** if $\mathbb{P}$ [$\forall \varepsilon > 0$, $\|X(k)\| > \varepsilon$ happens only finitely often] = 1. If sequences generated by a stochastic dynamical system converge to 0 almost surely, then the trivial solution $X(k) \equiv 0$ is **almost surely asymptotically stable**.

Note that almost sure convergence is also called convergence with probability one.

Definition 3.2. A random sequence $\{X(k) \in {}^n\}_{k=0}^{+\infty}$ **converges to 0 in the mean** if $\lim_{k\to\infty}\mathbb{E}[X(k)] = 0$ and **converges to 0 in the second moment** if $\lim_{k\to\infty}\mathbb{E}[X(k)X^{\mathrm{T}}(k)] = 0$. If sequences generated by a stochastic dynamical system converge to 0 in the mean or in the second moment, then the trivial solution $X(k) \equiv 0$ is **asymptotically stable in the mean or in the second moment,** respectively.

It can be shown that stability in the second moment implies stability in the mean, but in general, there is no relationship between second moment stability and almost sure stability. However, in the special case described by system (2.12) where $\mathbf{A}(k)$ are IID, stability in the second moment does imply almost sure stability; see [26]. We also remark that for vector valued sequences, defining moments higher than 2 is not trivial and they are rarely used in the literature; see [43].

We begin by characterizing the dynamics of the mean $\mathbb{E}[Y(k)]$ for (2.12). As explained below, stability of the mean provides a necessary condition for the stability of the stochastic system, that is, if the mean is unstable then the system is unstable. Therefore, the stability region for the mean in the parameter space contains the true stable region. We will then derive the dynamics of the second moment $\mathbb{E}[Y(k)Y^{\mathrm{T}}(k)]$ to provide sufficient conditions for almost sure stability.

Since $\mathbf{A}(k)$ is IID, it is independent of $Y(k)$. Thus, taking the expected value of both sides of (2.12), we obtain

$$\begin{aligned}[Y(k+1)]&=[\mathbf{A}(k)Y(k)]=[\mathbf{A}(k)][Y(k)]\\&=\left(\sum_{j=1}^{J}[\mathbf{A}(k)=\mathbf{A}_j]\mathbf{A}_j\right)[Y(k)]\\&=\left(\sum_{j=1}^{J}w_j\mathbf{A}_j\right)[Y(k)].\end{aligned} \tag{3.1}$$

Using the notation

Author Manuscript Author Manuscript Author Manuscript Author Manuscript

$$\overline{Y}(k) := [Y(k)] \in {}^{(r_J+1)n}, \quad (3.2)$$

we can write the discretized mean dynamics (3.1) in the form

$$\overline{Y}(k+1)=\overline{\mathbf{A}Y}(k), \quad (3.3)$$

where

$$\overline{\mathbf{A}}=\sum_{j=1}^{J} w_j \mathbf{A}_j=\sum_{j=1}^{J} w_j (\mathbf{G}_j)^{\ell}, \quad (3.4)$$

and $\overline{\mathbf{A}} \in \mathbb{R}^{(r_J+1)n\times(r_J+1)n}$, cf. (2.13). Thus, $\lim_{k\to\infty} \overline{Y}(k) = 0$ if and only if $\rho(\overline{\mathbf{A}}) < 1$, where $\rho(.)$ denotes the spectral radius. This is in fact a necessary condition for the stability of the stochastic system (2.12), which is the discretization of the continuous-time system (2.2).

To analyze the second moment of (2.12), we proceed as follows

$$\begin{aligned}
[Y(k+1)Y^{\mathrm{T}}(k+1)] &= [\mathbf{A}(k)Y(k)Y^{\mathrm{T}}(k)\mathbf{A}^{\mathrm{T}}(k)] \\
&= \sum_{j=1}^{J} [\mathbf{A}(k)=\mathbf{A}_j][\mathbf{A}(k)Y(k)Y^{\mathrm{T}}(k)\mathbf{A}^{\mathrm{T}}(k)|\mathbf{A}(k)=\mathbf{A}_j] \\
&= \sum_{j=1}^{J} w_j \mathbf{A}_j [Y(k)Y^{\mathrm{T}}(k)|\mathbf{A}(k)=\mathbf{A}_j]\mathbf{A}_j^{\mathrm{T}} \\
&= \sum_{j=1}^{J} w_j \mathbf{A}_j [Y(k)Y^{\mathrm{T}}(k)]\mathbf{A}_j^{\mathrm{T}},
\end{aligned} \quad (3.5)$$

where in the last step we used the independence of $Y(k)$ and $\mathbf{A}(k)$. Now we rewrite (3.5) as the time evolution of a vector. For a matrix $\mathbf{H} = [h_1\ h_2 \cdots h_m] \in \mathbb{R}^{n\times m}$, where $h_i \in \mathbb{R}^n$ denotes the i-th column vector, let us define the operator

$$\mathrm{vec}(\mathbf{H})= \begin{bmatrix} h_1 \\ h_2 \\ \vdots \\ h_m \end{bmatrix} \in {}^{nm}. \quad (3.6)$$

Using (3.6), let us define the vector

Author Manuscript Author Manuscript Author Manuscript Author Manuscript

$$\overline{\overline{Y}}(k) := \mathrm{vec}([Y(k)Y^{\mathrm{T}}(k)]) \in {}^{(r_J+1)^2n^2}, \quad (3.7)$$

and also note that for matrices **A**, **B**, and **C** for which the matrix product **ABC** is defined, the equality

$$\mathrm{vec}(\mathbf{ABC}) = (\mathbf{C}^{\mathrm{T}} \otimes \mathbf{A})\mathrm{vec}(\mathbf{B}) \quad (3.8)$$

holds, where ⊗ denotes the Kronecker product. Using (3.7) and (3.8), (3.5) can be rewritten as

$$\overline{\overline{Y}}(k+1) = \overline{\overline{\mathbf{A}}}\,\overline{\overline{Y}}(k), \quad (3.9)$$

where

$$\overline{\overline{\mathbf{A}}} = \sum_{j=1}^{J} w_j \mathbf{A}_j \otimes \mathbf{A}_j = \sum_{j=1}^{J} w_j (\mathbf{G}_j)^{\ell} \otimes (\mathbf{G}_j)^{\ell}, \quad (3.10)$$

and $\overline{\overline{\mathbf{A}}} \in \mathbb{R}^{(r_J+1)^2 n^2 \times (r_J+1)^2 n^2}$, cf. (2.13). Thus from (3.9), $\lim_{k\to\infty} \overline{\overline{Y}} = 0$ if and only if $\rho(\overline{\overline{\mathbf{A}}}) < 1$. Moreover, condition $\rho(\overline{\overline{\mathbf{A}}}) < \mathbf{1}$ implies almost sure stability of the stochastic system (2.12), which is the discretization of the continuous-time system (2.2). We remark that, if $J = 1$, conditions $\rho(\overline{\mathbf{A}}) < 1$ and $\rho(\overline{\overline{\mathbf{A}}}) < \mathbf{1}$ reduce to the asymptotic stability condition of a deterministic system with one single delay.

Remark 1. We provided stability conditions for the mean and the second moment of the map (2.12) that is a discretization of the continuous-time system (2.2). For the case of a deterministic delay, the semi-discretization method preserves asymptotic stability, i.e., if the original continuous-time system is stable, the discretized system is stable as well given that the time step Δt is small enough. Moreover, when Δt approaches zero, the stable parameter domain of the discretized system approaches the stable parameter domain of the continuous-time system; see [16, 17]. In the case of stochastic delay, our conjecture is that the stable parameter domain of the discretized system (2.12) converges to that of the continuous-time system (2.2) as $\Delta t \to 0$. The convergence proof may be constructed based on the fact that in the stochastic system the delay remains constant in each holding interval $[kT, (k+1)T)$, $k = 0,1,2,\ldots$, allowing one to apply the same arguments as in [16]. In this paper, we demonstrate the convergence through the spectral radius of matrices $\overline{\mathbf{A}}$ in (3.4) and $\overline{\overline{\mathbf{A}}}$ in (3.10) and corresponding stability charts.

Author Manuscript Author Manuscript Author Manuscript Author Manuscript

3.1. Convergence of Spectra and Stability Charts – An Illustrative Example

We consider a simple example in order to illustrate the stability analysis established in the previous section. By calculating the spectra of matrices (3.4) and (3.10) we draw stability charts. We also show that the spectral radius and the stability charts converge to a limit as the discretization step Δt decreases. Consider the scalar example $x \in \mathbb{R}$ in which case system (2.2) simplifies to

$$\dot{x}(t)=ax(t)+bx(t-\tau(t)), \quad (3.11)$$

where a and b are scalars. Assume that the delay may take the values $\tau_1 = 0.2$, $\tau_2 = 0.3$, and $\tau_3 = 0.4$ ($J = 3$) with equal probability, i.e., $w_1 = w_2 = w_3 = 1/3$, and set the holding time to $T = 0.1$. We draw stability charts in the plane of parameters a and b for different values of Δt. Note that here the matrix (2.11) simplifies to

$$\mathbf{G}_j=\begin{bmatrix} \alpha & 0 & \cdots & \beta & \cdots & 0 \\ 1 & 0 & 0 & \cdots & 0 & 0 \\ 0 & 1 & 0 & \cdots & 0 & 0 \\ 0 & 0 & 1 & \cdots & 0 & 0 \\ \vdots & \vdots & \vdots & \ddots & \vdots & \vdots \\ 0 & 0 & 0 & \cdots & 1 & 0 \end{bmatrix} \in {}^{(r_3+1)\times(r_3+1)}, \quad (3.12)$$

where $r_3 = \lfloor \tau_3/\Delta t \rfloor$ and

$$\alpha=\mathrm{e}^{a\Delta t}, \beta=(\mathrm{e}^{a\Delta t}-1)\frac{b}{a}, \quad (3.13)$$

cf. equation (2.9).

For comparison, first we consider stability analysis of the continuous-time mean dynamics

$$\dot{\bar{x}}(t)=a\bar{x}(t)+b\sum_{j=1}^{3} w_j \bar{x}(t-\tau_j), \quad (3.14)$$

(cf. (2.5) that holds since $T < \tau_1$). When using the trial solution $\bar{x}(t) = k\mathrm{e}^{st}$, $k, s \in \mathbb{C}$, we obtain the characteristic equation

$$s-a-b\sum_{j=1}^{3} w_j \mathrm{e}^{-s\tau_j}=0. \quad (3.15)$$

Author Manuscript Author Manuscript Author Manuscript Author Manuscript

Here, two different kinds of stability losses may occur: (i) a real eigenvalue crosses the imaginary axis at 0 (referred to as fold stability loss) corresponding to the boundary

$$b = -a, \quad (3.16)$$

(ii) a pair of complex conjugate eigenvalues crosses the imaginary axis at $\pm i\omega$ (referred to as Hopf stability loss) corresponding to the stability boundary

$$a = \frac{w\sum_{j=1}^{3} w_j \cos(\omega\tau_j)}{\sum_{j=1}^{3} w_j \sin(\omega\tau_j)}, \quad b = \frac{-\omega}{\sum_{j=1}^{3} w_j \sin(\omega\tau_j)}. \quad (3.17)$$

The boundaries (3.16) and (3.17) are obtained by substituting $s = 0$ and $s = i\omega$ into the characteristic equation (3.15). The parameter ω is varied continuously to obtain the Hopf stability bound (3.17). The stability curves corresponding to (3.16) and (3.17) are plotted as dashed black curves in Fig. 3.1.

In order to evaluate the stability of the discretized mean dynamics, given by equations (3.3) and (3.4), we consider the characteristic equation

$$\det(z\bar{\mathbf{I}} - \overline{\mathbf{A}}) = 0. \quad (3.18)$$

where $\bar{\mathbf{I}}$ is the $(r_3 + 1)$-dimensional identity matrix. This equation has $r_3 + 1 = \lfloor \tau_3/\Delta t \rfloor + 1$ solutions for the eigenvalues z. To investigate stability bounds in the (a, b) parameter space, we note that there can be three different kinds of stability losses defined by the movement of eigenvalues across the unit circle: (i) A real eigenvalue crosses the unit circle at 1; (ii) a real eigenvalue crosses the unit circle at −1; (iii) a pair of complex conjugate eigenvalues crosses the unit circle at $e^{\pm i\phi}$, $\phi \in (0, \pi)$. We refer to these as fold, flip, and Hopf stability losses, respectively, based on the nomenclature of the corresponding bifurcations of nonlinear systems. (A Hopf bifurcation for discrete-time systems is often called a Neimark-Sacker bifurcation.) To obtain the corresponding stability curves in cases (i) and (ii), we substitute $z = 1$ and $z = -1$ into the characteristic equation (3.18) and solve for b as a function of a. This may not be obtained analytically so we use numerical continuation to obtain the solution; see [44]. First we fix a, then consider an initial guess for b, and then correct it by using the Newton-Raphson method. Next we use this solution as an initial guess for a nearby value of a. This way we can continue the solution while varying a. In case (iii), we substitute $z = e^{i\phi}$ into the characteristic equation (3.18), separate the real and imaginary parts, and solve the equations for a and b as a function of ϕ. Again, we use numerical continuation to trace the curves in the (a, b)-plane while varying ϕ.

Author Manuscript Author Manuscript Author Manuscript Author Manuscript

The corresponding curves are plotted on the (a, b) parameter plane in the left column of Fig. 3.1 for different values of Δt as indicated. The dashed blue curve corresponds to fold stability loss, the solid blue curve corresponds to Hopf stability loss, and the equilibrium is mean stable in all shaded domains. The corresponding angular frequency $\omega = \phi/T$ increases along the Hopf curve when moving away from the dashed blue curve. Notice that as Δt decreases the boundary moves but it converges to the dashed black curve. The convergence can be further observed by looking at the eigenvalues in the second column of Fig. 3.1 corresponding to the point P located at (a, b) = (−1, −6.5). Indeed the number of eigenvalues increases but the leading eigenvalues converge with decreasing Δt while more and more eigenvalues appear in the vicinity of the origin. To better visualize the convergence of the leading eigenvalues we plot the spectral radius of $\bar{\mathbf{A}}$ as a function of $1/\Delta t$ in Fig. 3.2(a). We also calculate the leading eigenvalues of the continuous-time mean dynamics (3.14) from the characteristic equation (3.15) using the package DDEbiftool [8] for point P; these are $s_{1,2} = -0.037102 \pm i5.781085$. Then the corresponding leading eigenvalues of $\bar{\mathbf{A}}$ shall converge to $z_{1,2} = e^{s_{1,2}T}$ as $\Delta t \to 0$ and consequently $\rho(\bar{\mathbf{A}})$ converges to $|e^{s_{1,2}T}| = 0.996297$ that is shown in Fig. 3.2(a) as a dashed horizontal red line. Note that while the parameters α and β depend on Δt in matrix $\mathbf{G}j$ in (3.12), the size of the matrix $\mathbf{G}_j$ is also proportional to $1/\Delta t$. Therefore, we see discontinuities in the spectral radius of $\bar{\mathbf{A}}$ as Δt changes. We also remark that no flip instability can appear in the continuous-time system (3.14). If it were to appear in the corresponding discretized system, then the corresponding curve would have moved to infinity when taking the limit $\Delta t \to 0$. We remark further that in the case $T > \tau_1$ we still observe that the leading eigenvalues converge to a limit as $\Delta t \to 0$ but the mean dynamics are not anymore described by system (3.14) in the continuous limit.

To evaluate the stability of the second moment, we use (3.9) and (3.10)) and study the characteristic equation

$$\det(z\bar{\bar{\mathbf{I}}} - \bar{\bar{\mathbf{A}}}) = 0. \quad (3.19)$$

where $\bar{\bar{\mathbf{I}}}$ is the $(r_3 + 1)^2$-dimensional identity matrix. Here we have $(r_3 + 1)^2 = (\lfloor \tau_3/\Delta t \rfloor + 1)^2$ solutions for the eigenvalues z. Again, one may investigate the three possible stability losses but it turns out that only fold type occurs in this case. The corresponding curves are plotted as red curves in the (a, b)-plane in the left column of Fig. 3.1 where the second moment stable region is indicated by dark gray shading. The eigenvalues of matrix $\bar{\bar{\mathbf{A}}}$ at point P are plotted in the right column, showing convergence of the leading eigenvalues with decreasing Δt. The corresponding spectral radius is plotted in Fig. 3.2(b). Due to our hardware limitations, the smallest value of Δt for which we could compute $\rho(\bar{\bar{\mathbf{A}}})$ was 0.005, since the size of $\bar{\bar{\mathbf{A}}}$ grows with $1/\Delta t^2$. More details about the computational limitations of the method are given in Section 4.1. In this case, while we do not have an equation to describe the continuous-time second moment dynamics, we still observe that the spectral radius of $\bar{\bar{\mathbf{A}}}$ converges to a limit.

Author Manuscript Author Manuscript Author Manuscript Author Manuscript

4. Stochastic delays in a gene regulatory network

To illustrate the methods above we analyze the stability of genetic circuits where a protein regulates its own production. The two major processes involved are called transcription and translation [6]. During transcription, a gene (a section of the DNA) is copied into messenger RNA (mRNA) one nucleotide at a time by an enzyme called RNA polymerase. Then during translation, ribosomes “read” the genetic code from the messenger RNA to sequentially assemble proteins from amino acids. That is, transcription and translation involve sequential biochemical reactions [2]. Although each individual reaction generally happens on a fast time-scale, the large number of reactions required and their sequential nature can result in significant delays [52]. Further processes, such as protein folding and modification, can also impact the time it takes to produce a fully mature protein [39, 40]. Proteins can regulate (activate or repress) the production of other proteins by binding to the promoter region of the corresponding genes. Here we study the case where a protein represses its own production as shown by the diagram in Fig. 4.1. It has been shown that this single feedback system may produce oscillatory behavior and that time delays play a crucial role in the dynamics [47]. We construct two different models: a simpler model where the mRNA dynamics are neglected and another one where they are included. These examples allow us to highlight nontrivial dynamics caused by the stochastic delay variations.

We begin by describing how delays arise in protein production. We model the sequential biochemical reactions involved in protein production by the chain of reactions

$$\begin{aligned} P_0 &\xrightarrow{c_1} P_1, \\ P_1 &\xrightarrow{c_2} P_2, \\ &\vdots \\ P_{N-1} &\xrightarrow{c_N} P_N, \end{aligned} \tag{4.1}$$

where P_i denotes the number of molecules in the i-th state of the process and N is the number of reactions in the chain. For example, one may consider P_0 as the transcription initiation state and P_N as the fully mature protein. The parameter c_i is the reaction rate of the i-th reaction and the probability of reaction i happening during the time interval $[t, t + \mathrm{d}t]$ is proportional to the firing rate c_i and the number of proteins P_{i-1} in the $(i - 1)$-th state.

In Appendix A we assume that the time elapsed between reactions are independent and exponentially distributed and we consider the simplification $c_i = c$ for $i = 1,\ldots, N$ and the initial condition $P_0 = 1$, $P_i = 0$, for $i = 1,\ldots, N$. Then we show that the stochastic delay i.e., the total time elapsed between the first reaction and the last reaction in system (4.1) follows the Erlang distribution

$$w_e(\sigma) = \frac{c^N \sigma^{N-1} \mathrm{e}^{-c\sigma}}{(N-1)!}; \tag{4.2}$$

Author Manuscript Author Manuscript Author Manuscript Author Manuscript

see also [11]. Numerically we find that equation (4.2) still describes the delay distribution well for different initial conditions. To demonstrate this we consider $N = 50$ reactions, $c = 5$ reactions per second, the initial condition $P_0 = 10000$, $P_i = 0$, for $i = 1,\ldots, N$, and we simulate the reactions using a Gillespie algorithm [14]. The corresponding normalized histogram of the delay is overlaid with the distribution (4.2) in Fig. 4.2(a). We remark that in this case we still measure the delay as the time difference between the first reaction and the N-th reaction rather than tracing individual molecules in the simulation.

To characterize the Erlang distribution (4.2) we calculate its mean

$$E := \int_0^\infty w_{\mathrm{e}}(\sigma)\sigma \mathrm{d}\sigma = \frac{N}{c}, \quad (4.3)$$

and variance

$$V := \int_0^\infty w_{\mathrm{e}}(\sigma)(\sigma - E)^2 \mathrm{d}\sigma = \frac{N}{c^2}. \quad (4.4)$$

Notice that the relative variance

$$R := \frac{V}{E^2} = \frac{1}{N}, \quad (4.5)$$

is inversely proportional to the number of reactions N but does not depend on the transcription rate c; see [1].

4.1. Single gene auto-regulatory network

After characterizing the stochastic delay arising from sequential reactions we analyze the auto-repressor depicted in Fig. 4.1. Neglecting the mRNA dynamics, we consider the one-dimensional model

$$\dot{p}(t) = -\gamma p(t) + \frac{\kappa}{1 + (p(t - \tau(t))/p_{\mathrm{h}})^2}, \quad (4.6)$$

where p denotes the concentration of fully matured proteins. The linear term on the right hand side accounts for the protein degradation while the nonlinear term represents the protein production. Here, γ denotes the degradation rate, κ is the maximum production rate, and p_{h} is the protein concentration corresponding to half repression. The nonlinearity is in the form of a Hill function where the power 2 in the denominator represents repression strength. This model has been studied in the literature [6, 47] with constant delay $\tau(t) \equiv \tau$

Author Manuscript Author Manuscript Author Manuscript Author Manuscript

and can be shown to admit one of two behaviors: asymptotic convergence to a positive equilibrium or convergence to a limit cycle [33] depending on the parameters γ, κ, and p_h. Here, we assume that the delay follows a stationary stochastic process with Erlang distribution (4.2) and show that this system demonstrates similar behavior in the stochastic sense. More details about the reactions involved in system (4.6) can be found in Appendix B where the parameters γ, κ, and p_h are related to reaction rates using mass action kinetics. For the stability charts shown in the following section we set $p_h = 100$ proteins per cell and vary γ and κ while assuming $\gamma > 0$ and $\kappa > 0$.

The model (4.6) has a unique equilibrium $p(t) = p_*$ where p_* is the real solution of the cubic equation

$$p_*^3 + p_h^2 p_* - \frac{\kappa p_h^2}{\gamma} = 0. \quad (4.7)$$

To study the stability of this equilibrium, we define the perturbation $x(t) = p(t) - p_*$ and linearize the system (4.6) about the equilibrium. This yields

$$\dot{x}(t) = ax(t) + bx(t - \tau(t)), \quad (4.8)$$

with

$$a = -\gamma, \qquad b = \frac{-2\kappa p_h^2 p_*}{(p_h^2 + p_*^2)^2}. \quad (4.9)$$

Indeed, equation (4.8) has the same form as equation (3.11) but here the delay follows the Erlang distribution (4.2) instead of the uniform distribution used in Sec. 3.1.

As mentioned above, if the autocorrelation of the delay becomes zero after T and $T < \tau_{min}$ then we can use equation (2.6) to obtain the continuous-time mean dynamics. While $\tau_{min} = 0$ for the Erlang distribution, for the examples considered in this section the distribution is very close to zero for $\sigma \leq E - 3\sqrt{V}$; see Fig. 4.2(a) as an example and also Appendix A for some quantitative details. Thus, we assume $T < E - \sqrt{V}$ and we apply equation (2.6) with continuous distribution (4.2). Using the trial solution $\bar{x}(t) = ke^{st}$, $k, s \in \mathbb{C}$, we obtain the characteristic equation

$$s - a - b\frac{c^N}{(s+c)^N} = 0, \quad (4.10)$$

Author Manuscript Author Manuscript Author Manuscript Author Manuscript

which has finitely many (i.e., $N+1$) solutions for the eigenvalues s. It can be shown that when the Erlang distribution is perturbed with perturbation size ε, additional spectra appear in the neighborhood of these eigenvalues such that the size of the neighborhood is proportional to ε. Additional eigenvalues may also appear to the left of a vertical line located at Res$= -1/\varepsilon$; see [10].

Again we check for two types of stability losses. Substituting $s = 0$ into equation (4.10) still results in $b = -a$ but when using equations (4.7) and (4.9) no feasible solutions can be found in the (γ, κ) parameter plane. On the other hand, when substituting $s = \mathrm{i}\omega$ into equation (4.10) we obtain the stability boundary

$$\begin{aligned} a &= \frac{\omega \cos(N\theta)}{\sin(N\theta)}, \\ b &= \frac{-\omega}{\sin(N\theta)} \left(1 + \frac{\omega^2}{c^2}\right)^{\frac{N}{2}}, \end{aligned} \tag{4.11}$$

where

$$\theta = \tan^{-1}\left(\frac{\omega}{c}\right). \tag{4.12}$$

Now using equations (4.7) and (4.9) one may obtain

$$\begin{aligned} \gamma &= -a, \\ \kappa &= -2p_{\mathrm{h}} \frac{a^2}{b} \left(\frac{b}{2a-b}\right)^{3/2}, \end{aligned} \tag{4.13}$$

which do result in a stability curve in the positive quadrant in (γ, κ)-plane; see black dashed curves in Fig. 4.3.

In order to apply the stability analysis developed in Section 3, the delay distribution must have finite support. To achieve this we truncate and discretize the Erlang distribution $w_{\mathrm{e}}(\sigma)$ given in (4.2). Again, noticing that the distribution is close to zero when σ is more than three standard deviations away from the mean, we set weights at $\sigma_i = E - 3\sqrt{V} + (i-1)\Delta t$ to be

$$\tilde{w}_i = \begin{cases} \Delta t w_e(\sigma_i), & \text{if } |\sigma_i - E| \leq 3\sqrt{V} \\ 0, & \text{if } |\sigma_i - E| > 3\sqrt{V} \end{cases} \tag{4.14}$$

for $i = 1, 2, \ldots$ such that $\tilde{w_i} \neq 0$ only for $i = q, \ldots, Q$. Finally, we normalize the distribution by

Author Manuscript Author Manuscript Author Manuscript Author Manuscript

$$w_j = \frac{\tilde{w}_{q+j-1}}{\sum_{k=q}^{Q} \tilde{w}_k}, \quad (4.15)$$

for $j = 1,\ldots, J$ where $J = Q - q + 1$. Fig. 4.2(b) depicts the discretization of the Erlang distribution shown in Fig. 4.2(a) with $\Delta t = 1$ [s].

Once the delay distribution w is characterized for system (4.8),(4.9), we may construct the discretized systems (3.3),(3.4) for the mean and (3.9),(3.10) for the second moment to analyze their stability using the characteristic equations (3.18) and (3.19), respectively. The results are shown in Fig. 4.3 in the (γ, κ) parameter plane where the same notation is used as in the left column of Fig. 3.1. We vary the mean E and the relative variance R, as indicated, in order to understand the effects of changing the probability distribution of the delay. Note that the delay distribution used in Fig. 4.3(g) corresponds to the case shown in Fig. 4.2(b). We kept Δt constant for all the plots in Fig. 4.3 so that the effect of changing the delay values is reflected accurately. When we discretize the continuous delay distribution (4.2), we use the same time step as the time discretization step Δt. In all the panels in Fig. 4.3, we set $\Delta t = 1$[s] and also $T = 1$[s].

As explained above, the mean loses stability only via Hopf stability loss where the angular frequency ω increases along the stability boundary from left to right (blue curves obtained by the semi-discretization and the black dashed curves obtained through (4.10)-(4.13)). For the second moment, only fold stability loss occurs and the corresponding red curves are obtained by the semi-discretization. In general, the stability regions shrink when increasing the mean delay $E = N/c$ and when decreasing relative variance $R = 1/N$. Also, when decreasing R the difference between mean stability and second moment stability decreases as indicated by the size of the light gray area. This corresponds to the fact that as the delay distribution is getting narrower, the dynamics get closer to the dynamics of a system with a single delay $\tau \equiv E$. Moreover, notice that the size of the dark gray domain, where the second moment is stable, increases with R indicating that the stochasticity in the delay may stabilize the system. Similar results relating to noise induced stability have been shown in other works [3, 4, 27, 32].

We remark that our stability analysis may require large computational effort when calculating the largest eigenvalues of the matrix $\bar{\bar{\mathbf{A}}}$ in (3.10). This may cause problems especially if both large and small delays exist in the system. In particular, Δt should be smaller than the minimum delay $\tau_{\min}$ in the system so that $\left\lfloor \frac{\tau_{\min}}{\Delta t} \right\rfloor \geq 1$. Otherwise all the delays that are smaller than Δt will be neglected in the analysis. On the other hand, if $\tau_{\max} \gg \tau_{\min}$ the size of matrix $\bar{\bar{\mathbf{A}}}$, that is proportional to $\left(\left\lfloor \frac{\tau_{\max}}{\Delta t} \right\rfloor \right)^2$, gets unmanageably large. In panels (b-d) and (f-h), $\Delta t = 1$[s] is small enough. Consequently, the blue curves obtained by the semi-discretization approximate well the black dashed curves obtained using the continuous-time mean dynamics (4.11)-(4.13). On the other hand for the wide distributions

Author Manuscript Author Manuscript Author Manuscript Author Manuscript

used in Fig. 4.3(a,e), $\Delta t = 1$[s] is not small enough. In particular, in case (a), we have $\tau_{\min} = E - 3\sqrt{V} \approx 0.26$. Therefore ideally Δt should be smaller than 0.26.

In order to demonstrate the time evolution of the linear system (4.8),(4.9) and the original nonlinear system (4.6), we use numerical simulation that is based on semi-discretization, i.e., we assume the delayed term stays constant in the time interval $[i\Delta t, (i+1)\Delta t]$. Since in (4.6), the delayed term is contained in the only nonlinearity, the resulting ODE can still be solved analytically in each interval. The Erlang distribution is also discretized as in (4.14)-(4.15). We set $E = 10$ [s] and $R = 0.02$ and choose three points marked with A ($\gamma = 1.5$, $\kappa = 600$), B ($\gamma = 2.5$, $\kappa = 600$), and C ($\gamma = 3.5$, $\kappa = 600$) in different regions in Fig. 4.3(g). The initial condition is set to $x(t) \equiv 0.1p_*$ in the linear system (4.8) (that corresponds to $p(t) \equiv 1.1p_*$ in the nonlinear system (4.6)) along the time domain $t \in [-\tau_f, 0]$ where p_* is the equilibrium obtained from (4.7).

The results are summarized in Fig. 4.4 where the black curve indicates the mean and the red curves bound the mean plus and minus the standard deviation computed from 1000 simulations. A sample realization is shown by a gray curve in each panel. Fig. 4.4(a–c) show the results for the linear system (4.8),(4.9). In case A, the equilibrium is unstable and both the mean and the standard deviation diverge. In case B, the mean converges to zero while the standard deviation diverges. In case C, both the mean and the standard deviation converge to zero corresponding to almost sure stability of the equilibrium. The corresponding simulation results for the nonlinear system (4.6) are displayed in Fig. 4.4(d–f). The results are qualitatively similar to the linear ones except that in cases A and B the standard deviation does not go to infinity but saturates due to the saturating nonlinear terms. The corresponding nonlinear oscillations shown by the gray sample trajectories resemble those found for a deterministic system with distributed delay in [33]. For example, by doing Fast Fourier Transform (FFT) analysis, the main frequency of the nonlinear oscillations is found to be close to the Hopf frequency at which the continuous-time mean dynamics lose stability. Note that in case C, almost sure stability of the equilibrium is ensured by our analysis at the linear level only, but the nonlinear system also demonstrates almost sure stability.

4.2. A single gene auto-regulatory network with mRNA dynamics and dual delayed feedback

We now consider a model where we incorporate mRNA dynamics, resulting in a non-scalar example. Additionally, we assume that the system has two distinct regulatory pathways with distinct signaling delays [31, 50].

In particular, we consider the model

$$\begin{aligned} \dot{\hat{m}}(t) &= -\gamma_m \hat{m}(t) + \frac{\alpha_m}{1+(p(t-\tau(t))/p_h)^2} \\ \dot{p}(t) &= -\gamma_p p(t) + \alpha_p \hat{m}(t), \end{aligned} \tag{4.16}$$

where $\hat{m}$ is the concentration of mRNA in the transcriptional initiation phase, p is the concentration of fully matured protein, and γ_m and γ_p are mRNA and protein degradation

Author Manuscript Author Manuscript Author Manuscript Author Manuscript

rates, respectively. The nonlinear term in the first equation in (4.16) incorporates the feedback due to self-repression where the delay $\tau(t)$ still represents the total delay in the feedback loop and α_m is the maximum mRNA production rate. According to the second equation in (4.16), the protein production is assumed to be proportional to the mRNA concentration with rate α_p. Assuming that mRNA dynamics are fast relative to the protein dynamics, i.e., assuming that the first equation in (4.16) approaches steady state quickly, the model (4.16) can be reduced to (4.6) with $\kappa = \alpha_p\alpha_m/\gamma_m$ as shown in Appendix B.

As mentioned above, we assume two distinct signaling pathways. Thus, the delay $\tau(t)$ will have a bimodal distribution where each mode resembles an Erlang distribution. To simplify the model we consider a bimodal distribution with two distinct delay values τ_1 and τ_2, that is, the probability density function

$$w(\sigma)=u\delta(\sigma-\tau_1)+(1-u)\delta(\sigma-\tau_2), \quad (4.17)$$

where $0 \le u \le 1$ represents the likelihood of the protein being produced through pathway 1 and it can be tuned through a combination of relative plasmid copy numbers, promoter strengths, and ribosome binding strengths. The steady state protein concentration is the real solution of the cubic equation

$$p_*^3+p_{\rm h}^2p_*-\frac{\alpha_m\alpha_p p_{\rm h}^2}{\gamma_m\gamma_p}=0, \quad (4.18)$$

that is the equilibrium point of (4.16) is the same as that of (4.6) since $\kappa = \alpha_m\alpha_p/\gamma_m$. The steady state mRNA concentration is $m_* = (\gamma_p/\alpha_p)p_*$. Defining the perturbation $x = [\hat{m} - m_* \; p - p_*]$, we linearize (4.16) around the steady state obtaining the form (2.2) with matrices

$$\mathbf{a}=\begin{bmatrix} -\gamma_m & 0 \\ \alpha_p & -\gamma_p \end{bmatrix}, \mathbf{b}=\begin{bmatrix} 0 & \frac{-2\kappa p_{\rm h}^2 p_*}{(p_{\rm h}^2+p_*^2)^2} \\ 0 & 0 \end{bmatrix}. \quad (4.19)$$

Figure 4.5(a−c) show stability plots for different values of the parameter u of the distribution (4.17). The delay holding time is assumed to be $T = 5$ [s] and a time step of $\Delta t = 1$ [s] is used for the semi-discretization. Figure 4.5(a) and (b) show the second moment stable region (the dark grey shaded area) for $u = 1$ and $u = 0$, respectively. The values $u = 1$ and $u = 0$ correspond to the deterministic systems with delays $\tau = 10$ and $\tau = 20$, respectively. Figure 4.5(c) shows the stable region for the stochastic system with $u = 0.75$.

We mark point Q at $(\gamma_p, \alpha_m) = (0.5, 70)$ in the parameter space, which pertains to instability of system (4.16) for the single delay feedback with $\tau = 10$ [s] and $\tau = 20$ [s]. However, our stability analysis predicts a stable system for $u = 0.75$ where the delay stochastically varies between these two values. Fig. 4.5(d–f) shows the simulations of the nonlinear model (4.16)

Author Manuscript Author Manuscript Author Manuscript Author Manuscript

where the protein concentration is shown as a function of time for the parameter values associated with point Q. In panels (d) and (e), the simulations with a single deterministic delay $\tau = 10$ and $\tau = 20$ are shown, respectively In these cases, the equilibrium point is unstable and we see oscillations in the protein concentration. Panel (f) shows the simulation when the delay varies stochastically between the two values with $u = 0.75$ and holding time $T = 5$ [s]. In this case, the equilibrium becomes stable. We used the semi-discretization to simulate the continuous-time nonlinear system (4.16) with the parameters $\gamma_m = 0.25 \left[\frac{1}{\mathrm{s}}\right]$, $\alpha_p = 1 \left[\frac{1}{\mathrm{s}}\right]$, $p_h = 100$ proteins per cell, and initial conditions $\hat{m}(\xi) = 1.1 m_*$, $p(\xi) = 0.2 p_*$ for $-\tau_{\max} \le \xi \le 0$.

Fig. 4.6(a) shows the spectral radius of matrix $\bar{\bar{\mathbf{A}}}$ as a function of the distribution parameter u. Notice that as u decreases from 1 to 0 the spectral radius initially decreases (that is, the stable regime grows), but then begins to increase again (the stable regime shrinks again). In the parameter regime $0.59 < u < 0.88$ the stochastic system is stable. Fig. 4.6(b) shows the spectral radius of matrix $\bar{\bar{\mathbf{A}}}$ as a function of the holding time T. It is seen that system (4.16) can be destabilized by increasing the delay holding time T. This may be explained noting that for large T values the system dwells in an unstable system pertaining to each delay value. The dynamics are only stabilized by the switching events between the two unstable systems.

5. Conclusion and Discussion

Delay differential equations with stochastic delay were investigated in this paper. In particular, we derived stability conditions for equilibria by analyzing the mean and the second moment dynamics. We showed that if the delay follows a stationary stochastic process with autocorrelation becoming zero fast enough, then the mean dynamics are described by a distributed delay system that can be analyzed to obtain necessary conditions for the stability of the stochastic system. We also used the notion of second moment stability to ensure almost sure stability. We applied the semi-discretization technique and demonstrated convergence of spectra and stability charts when decreasing the size of the discretization time step.

The theoretical tools were applied to simple auto-regulatory gene networks where stochastic delays appear due to sequential biochemical reactions. We showed that the resultant delay distribution is well approximated by an Erlang distribution. We first investigated an auto-regulatory gene circuit described by a scalar model. We found that increasing the stochasticity in the delay (characterized by the relative variance of the distribution) increased the size of the almost sure stable region indicating that stochasticity in the delay may stabilize unstable equilibria. Our findings were justified using numerical simulations of the linearized and full nonlinear system. We also investigated the auto-regulatory circuit taking into account mRNA dynamics which yielded a model with a higher dimension where we included a bimodal delay distribution. We found that even if both the regulatory delays are individually destabilizing, the stochastic combination of these two delays can make the system stable. Furthermore, we found that the longer the dwelling times, the more unstable

Author Manuscript Author Manuscript Author Manuscript Author Manuscript

the network became. We plan to use the developed tools to analyze the dynamics of more complicated synthetic and natural gene regulatory networks.

While we were able to derive mean dynamics in the continuous limit (when the autocorrelation of the delay became zero faster than the shortest delay), such limit was not found for the second moment dynamics analytically but left for future research. Moreover, we remark that the stochastic delay system studied in this paper can also be viewed as a hybrid system where switching between various delayed-differential equations happen in a stochastic fashion. Work has been done on the stability analysis of hybrid systems with constant time delays [30, 34, 53, 54] or with deterministically time-varying delays [42]; however, modeling stochastic delay systems such as ours is less explored in the hybrid systems literature.

Acknowledgments

The authors would like to thank Mark J. Balas for helpful discussion.

Marcella M. Gomez: The research of this author was supported by the TerraSwarm Research Center, one of six centers supported by the STARnet phase of the Focus Center Research Program (FCRP) a Semiconductor Research Corporation program sponsored by MARCO and DARPA.

Mehdi Sadeghpour, Gábor Orosz: This research was supported by National Science Foundation (award # 1300319).

Matthew R. Bennett: The research of this author was supported by the NIH, through the joint NSF/NIGMS Mathematical Biology Program grant R01GM104974, and the Robert A. Welch Foundation grant C-1729

Appendix A. Erlang distribution

In this appendix we provide some details about the derivation and properties of the Erlang distribution used in the main part of the paper. Consider the chain of reactions shown in equation (4.1), assuming that $c_1 = c_2 = \ldots = c_N = c$. That is,

$$\begin{aligned} p_0 &\xrightarrow{c} p_1, \\ p_1 &\xrightarrow{c} p_2, \\ &\vdots \\ p_{N-1} &\xrightarrow{c} p_N, \end{aligned} \quad \text{(A.1)}$$

where P_i represents the number of molecules of species i and we define the time delay τ as the time it takes for a molecule to go through this chain of reactions. Let us assume the initial conditions to be such that at time $t = 0$ we have $P_0 = 1$ and $P_i = 0$, $i = 1,\ldots, N-1$. The reactions are assumed to happen sequentially such that the first reaction happens at time t_1, the second reaction happens at time $t_1 + t_2$, and so forth. The last reaction happens at time $\sum_{k=1}^{N} t_k$ that is equal to the delay τ. Then, the state vector changes as

Author Manuscript Author Manuscript Author Manuscript Author Manuscript

$$\begin{matrix} \\ \begin{bmatrix} P_0 \\ P_1 \\ P_2 \\ \vdots \\ P_N \end{bmatrix} \end{matrix} \quad \begin{matrix} 0 \\ \begin{bmatrix} 1 \\ 0 \\ 0 \\ \vdots \\ 0 \end{bmatrix} \end{matrix} \quad \begin{matrix} t_1 \\ \begin{bmatrix} 0 \\ 1 \\ 0 \\ \vdots \\ 0 \end{bmatrix} \end{matrix} \quad \begin{matrix} t_1+t_2 \\ \begin{bmatrix} 0 \\ 0 \\ 1 \\ \vdots \\ 0 \end{bmatrix} \end{matrix} \quad \cdots \quad \begin{matrix} \sum_{k=1}^{N} t_k=\tau \\ \begin{bmatrix} 0 \\ 0 \\ 0 \\ \vdots \\ 1 \end{bmatrix} \end{matrix} \quad \text{(A.2)}$$

In chemical reaction networks, a fundamental assumption is to model reaction occurrence times as arrivals of a Poisson process [6]. Therefore, the time elapsed between reactions is an exponential random variable. The rate at which reaction i occurs is determined by the propensity cP_{i-1} and thus t_i is an exponential random variable with rate cP_{i-1}. Based on the state vectors shown in (A.2), the times t_i, $i = 1,\ldots, N$ are exponential random variables with identical rate c. Furthermore, we assume that they are independent. That is, the time delay $\tau=\sum_{k=1}^{N} t_k$ is the sum of N independent, exponentially-distributed random variables. To find the probability density function of τ we start with introducing the notation $\tilde{t} := \sum_{k=2}^{N} t_k$. Thus the cumulative distribution function becomes

$$F_N(t)=[\tau<t]=[t_1+\tilde{t}<t]=\int_0^\infty [t_1+\tilde{t}<t|t_1=u]ce^{-cu}du, \quad \text{(A.3)}$$

Moreover,

$$[t_1+\tilde{t}<t|t_1=u]=\begin{cases} 0, & \text{if } u \geq t, \\ [\tilde{t}<t-u|t_1=u]=[\tilde{t}<t-u], & \text{if } u<t, \end{cases} \quad \text{(A.4)}$$

where we used independence of t_1 and $\tilde{t}$. Also, $F_{N-1}(t-u) = \mathbb{P}[\tilde{t} < t-u]$ since $\tilde{t}$ is the sum of $N-1$ independent, exponentially-distributed random variables. Substituting this into (A.3) and (A.4) we obtain the recursive rule

$$F_N(t)=\int_0^t ce^{-cu}F_{N-1}(t-u)du. \quad \text{(A.5)}$$

Taking the derivative of both sides with respect to time t, we obtain a similar relationship between the probability density functions

$$w_N(t)=\int_0^t ce^{-cu}w_{N-1}(t-u)du, \quad \text{(A.6)}$$

Author Manuscript Author Manuscript Author Manuscript Author Manuscript

where $w_k(t)=\frac{\mathrm{d}}{\mathrm{d}t}F_k(t)$, $k = 1,\ldots, N$.

Now we show by induction that the probability density function $w_N(t)$ follows the Erlang distribution (4.2). For $N = 1$ we have

$$F_1(t)=[t_1<t]=\int_0^t c\mathrm{e}^{-cu}\mathrm{du}=1-\mathrm{e}^{-ct}\Rightarrow w_1(t)=\frac{\mathrm{d}}{\mathrm{d}t}F_1(t)=c\mathrm{e}^{-ct}. \quad \text{(A.7)}$$

Assume $w_{N-1}(t)$ is Erlang. Thus using (A.6), we have

$$w_N(t)=\int_0^t c\mathrm{e}^{-cu}\frac{c^{N-1}(t-u)^{N-2}\mathrm{e}^{-c(t-u)}}{(N-2)!}\mathrm{d}u=\frac{c^N t^{N-1}\mathrm{e}^{-ct}}{(N-1)!}, \quad \text{(A.8)}$$

that completes the proof.

In the method proposed in the paper, we discretize the Erlang distribution such that we neglect the delays less than $E - n\sqrt{V}$ and larger than $E + n\sqrt{V}$ where E denotes the mean, V denotes the variance. We choose $n = 3$ for the examples shown in the paper. Here, we discuss this approximation and investigate other values of n.

The cumulative distribution function of the Erlang distribution (4.2) is

$$F_e(\tau)=\int_0^\tau w_e(\sigma)\mathrm{d}\sigma=1-\mathrm{e}^{-c\tau}\sum_{k=0}^{N-1}\frac{(c\tau)^k}{k!}. \quad \text{(A.9)}$$

Therefore, the probability of the delay falling between $E - n\sqrt{V}$ and $E + n\sqrt{V}$ is

$$[|\tau-E|<n\sqrt{V}]=F_e(E+n\sqrt{V})-F_e(E-n\sqrt{V}). \quad \text{(A.10)}$$

Substituting $E = N/c$ (cf. (4.3)) and $\sqrt{V}=\sqrt{N}/c$ (cf. (4.4)) into A.10 and assuming $E - n\sqrt{V} > 0$, we can show by some algebraic manipulations that

$$[|\tau-E|<n\sqrt{V}]=-e^{-(N+n\sqrt{N})}\sum_{k=0}^{N-1}\frac{(N+n\sqrt{N})^k}{k!}+\mathrm{e}^{-(N-n\sqrt{N})}\sum_{k=0}^{N-1}\frac{(N-n\sqrt{N})^k}{k!}. \quad \text{(A.11)}$$

If $E - n\sqrt{V} \leq 0$, we have

Author Manuscript Author Manuscript Author Manuscript Author Manuscript

$$[|\tau - E| < n\sqrt{V}] = F_e(E + n\sqrt{V}) - F_e(0) = 1 - e^{-(N+n\sqrt{N})} \sum_{k=0}^{N-1} \frac{(N+n\sqrt{N})^k}{k!}. \quad \text{(A.12)}$$

Table A.1

$\mathbb{P}[|\tau - E| < n\sqrt{V}]$ for different n and N values.

	$n = 1$	$n = 2$	$n = 3$	$n = 4$	$n = 5$
$N = 10$	0.69120	0.95851	0.99328	0.99899	0.99987
$N = 20$	0.68683	0.95688	0.99506	0.99946	0.99995
$N = 50$	0.68432	0.95553	0.99635	0.99974	0.99999
$N = 100$	0.68350	0.95503	0.99682	0.99984	0.99999

Note (A.11) or (A.12) only depend on N and n and Table A.1 shows the corresponding numerical values for different values of N and n. This shows that the probability of falling outside the domain $[E - n\sqrt{V}, E + n\sqrt{V}]$ is less than 1% for $n = 3$.

Appendix B. Mass-action kinetics of the auto-regulatory network

Here, we use mass-action kinetics to provide some details regarding the origin of the parameters such as degradation and production rates that appear in the auto-regulatory network models (4.6) and (4.16). We first consider mRNA dynamics into account to derive model (4.16). Then we show how one can simplify (4.16) to (4.6) using quasi steady state approximations (QSSA). We assume that the proteins produced through transcription and translation form dimers which bind to the promoter site of the gene and repress their own transcription by blocking the RNA polymerase from binding.

The set of reactions we consider are

$$\begin{aligned}
&P + P \underset{K_-}{\overset{k_+}{\rightleftharpoons}} D,\\
&G + D \underset{r_-}{\overset{r_+}{\rightleftharpoons}} G_{\mathrm{d}},\\
&G \xrightarrow{\nu} G + M_0,\\
&M_0 \xrightarrow{c} M_1,\\
&\vdots\\
&M_N \xrightarrow{c} M,\\
&M \xrightarrow{\gamma_m} \varnothing,\\
&M \xrightarrow{\tilde{\nu}} M + p_0,\\
&P_0 \xrightarrow{\tilde{c}} P_1,\\
&\vdots\\
&P_{\tilde{N}} \xrightarrow{\tilde{c}} P,\\
&P \xrightarrow{\gamma_p} \varnothing,
\end{aligned} \quad \text{(B.1)}$$

Author Manuscript Author Manuscript Author Manuscript Author Manuscript

where P represents the number of the fully mature proteins (often called transcription factors), M represents the number of mRNA transcripts, D is the number of dimers, G is the number of genes without dimers bound to them, and G_{d} is the number of genes with dimers bound.

Finally, the symbols M_i, $i = 0,\ldots, N$, and P_i, $i = 0,\ldots, \tilde{N}$ are the numbers of molecules of mRNA and protein in the intermediate stages of synthesis in the transcription and translation processes, respectively The variables k_+ and k_- are the associative and dissociative rate constants for dimerization, while r_+ and r_- are the reaction rates for binding and unbinding of a dimer to the promoter site. The initiation of the transcription that occurs when an RNA polymerase binds to a gene with an unoccupied promoter site occurs with reaction rate ν. For each reaction in the following sequence the reaction rate is set to c (transcription rate). The initiation of the translation occurs at rate $\tilde{\nu}$ and each reaction in the following sequence happens with rate $\tilde{c}$. The symbols γ_m and γ_p represent the mRNA and protein degradation rates, respectively. We remark that further details may be considered regarding the binding of the RNA polymerase [23] that are omitted here for simplicity.

Using the generalized mass-action kinetics for (B.1), we arrive at the following set of ODEs

$$\begin{aligned}
\tfrac{\mathrm{d}d}{\mathrm{d}t} &= k_+p^2 - k_-d - r_+gd + r_-g_{\mathrm{d}},\\
\tfrac{\mathrm{d}g}{\mathrm{d}t} &= -r_+gd + r_-g_{\mathrm{d}},\\
\tfrac{\mathrm{d}m_0}{\mathrm{d}t} &= \nu g - cm_0,\\
\tfrac{\mathrm{d}m_i}{\mathrm{d}t} &= cm_{i-1} - cm_i, \text{ for } i = 1,\ldots,N,\\
\tfrac{\mathrm{d}m}{\mathrm{d}t} &= -\gamma_m m + cm_N,\\
\tfrac{\mathrm{d}p_0}{\mathrm{d}t} &= \tilde{\nu}m - \tilde{c}p_0,\\
\tfrac{\mathrm{d}p_i}{\mathrm{d}t} &= \tilde{c}p_{i-1} - \tilde{c}p_i, \text{ for } i = 1,\ldots,\tilde{N},\\
\tfrac{\mathrm{d}p}{\mathrm{d}t} &= -\gamma_p p + \tilde{c}p_{\tilde{N}} - 2k_+p^2 + 2k_-d,
\end{aligned} \tag{B.2}$$

where the lower case letters denote the corresponding concentrations and the plasmid copy number $g + g_{\mathrm{d}}$ is assumed to be constant. Notice that the set of linear equations for m_i, $i = 1,\ldots, N$ and p_i, $i = 1,\ldots, \tilde{N}$ can be solved analytically to obtain $m_N(t)$ and $p_{\tilde{N}}(t)$ as a function of $m_0(t)$ and $p_0(t)$, respectively. In particular, considering zero initial conditions we have

$$m_i(t) = \int_0^t c\mathrm{e}^{-c(t-u)} m_{i-1}(u)\mathrm{d}u, \tag{B.3}$$

for $i = 1,\ldots, N$. Substituting the solution

$$m_1(t) = \int_0^t c\mathrm{e}^{-c(t-u)} m_0(u)\mathrm{d}u, \tag{B.4}$$

into the formula of $m_2(t)$ gives

Author Manuscript Author Manuscript Author Manuscript Author Manuscript

$$m_2(t)=\int_0^t c\mathrm{e}^{-c(t-v)}m_1(v)\mathrm{d}v=\int_0^t\int_0^v c^2\mathrm{e}^{-c(t-u)}m_0(u)\mathrm{d}u\mathrm{d}v=\int_0^t c^2\sigma\mathrm{e}^{-c\sigma}m_0(t-\sigma)\mathrm{d}\sigma, \quad \text{(B.5)}$$

where we changed the order of integration and defined the new variable $\sigma = t - u$ to obtain the result. Similarly, we can obtain

$$m_3(t)\int_0^t \frac{c^3\sigma^2\mathrm{e}^{-c\sigma}}{2!}m_0(t-\sigma)\mathrm{d}\sigma. \quad \text{(B.6)}$$

Repeating the integration in the same manner we arrive at

$$m_{_N}(t)=\int_0^\infty \frac{c^N\sigma^{N-1}\mathrm{e}^{-c\sigma}}{(N-1)!}m_0(t-\sigma)\mathrm{d}\sigma=\int_0^\infty w_{\mathrm{e}}(\sigma)m_0(t-\sigma)\mathrm{d}\sigma, \quad \text{(B.7)}$$

where $w_{\mathrm{e}}(\sigma)$ is the Erlang distribution (4.2) and we extended the integration limit to infinity since we consider $m_0(t) \equiv 0$ for $t \leq 0$. Similarly for $p_{\tilde{N}}(t)$ we have

$$p_{_{\tilde{N}}}(t)=\int_0^\infty \frac{\tilde{c}^{\tilde{N}}\sigma^{\tilde{N}-1}\mathrm{e}^{-\tilde{c}\sigma}}{(\tilde{N}-1)!}p_0(t-\sigma)\mathrm{d}\sigma=\int_0^\infty \tilde{w}_{\mathrm{e}}(\sigma)p_0(t-\sigma)\mathrm{d}\sigma, \quad \text{(B.8)}$$

where $\tilde{w}_{\mathrm{e}}(\sigma)$ is the Erlang distribution with order $\tilde{N}$ and rate $\tilde{c}$. Using (B.7) and (B.8), we can reduce (B.2) to

$$\begin{aligned}
\tfrac{\mathrm{d}d}{\mathrm{d}t}&=k_+p^2-k_-d-r_+gd+r_-g_{\mathrm{d}},\\
\tfrac{\mathrm{d}g}{\mathrm{d}t}&=-r_+gd+r_-g\mathrm{d},\\
\tfrac{\mathrm{d}m_0}{\mathrm{d}t}&=vg-cm_0,\\
\tfrac{\mathrm{d}m}{\mathrm{d}t}&=\gamma_m m+c\int_0^\infty w_{\mathrm{e}}(\sigma)m_0(t-\sigma)\mathrm{d}\sigma,\\
\tfrac{\mathrm{d}p_0}{\mathrm{d}t}&=\tilde{v}m-\tilde{c}p_0,\\
\tfrac{\mathrm{d}p}{\mathrm{d}t}&=-\gamma_p p+\tilde{c}\int_0^\infty \tilde{w}_{\mathrm{e}}(\sigma)p_0(t-\sigma)\mathrm{d}\sigma-2k_+p^2+2k_-d.
\end{aligned} \quad \text{(B.9)}$$

This may be further reduced by using quasi-steady state approximations and singular perturbation methods. In particular, assuming that the kinetics of dimerization, promoter binding, transcription initiation, and translation initiation happen on a fast time-scale, the corresponding equations can be assumed to reach equilibrium quickly, allowing us to replace $d(t)$, $g(t)$, $m_0(t)$, and $p_0(t)$ with their respective steady-state values yielding

Author Manuscript Author Manuscript Author Manuscript Author Manuscript

$$\begin{aligned}\dot{m}(t) &= -\gamma_m m(t) + \int_0^\infty w_e(\sigma) \frac{\alpha_m}{1+(p(t-\sigma)/p_h)^2} d\sigma, \\ \dot{p}(t) &= -\gamma_p p(t) + \int_0^\infty \tilde{w}_e(\sigma) \alpha_p m(t-\sigma) d\sigma,\end{aligned} \tag{B.10}$$

with constants $\alpha_m = \nu(g+g_d)$, $p_h = \sqrt{\frac{r_- k_-}{r_+ k_+}}$ and $\alpha_p = \tilde{\nu}$.

Note that equations (B.10) are the mean dynamics of the auto-regulatory network as they are obtained through mass-action kinetics. Thus we may assume a single delay $\bar{\sigma}$ for the transcription and a single delay $\tilde{\bar{\sigma}}$ for the translation to obtain

$$\begin{aligned}\dot{m}(t) &= -\gamma_m m(t) + \frac{\alpha_m}{1+(p(t-\bar{\sigma})/p_h)^2}, \\ \dot{p}(t) &= -\gamma_p p(t) + \alpha_p m(t-\tilde{\bar{\sigma}}).\end{aligned} \tag{B.11}$$

We can further simplify (B.11) by using the change of variables $\hat{m}(t) = m(t-\tilde{\bar{\sigma}})$. This allows us to absorb the two delays into one single delay $\tau = \bar{\sigma} + \tilde{\bar{\sigma}}$ and change (B.11) to

$$\begin{aligned}\dot{\hat{m}}(t) &= -\gamma_m \hat{m}(t) + \frac{\alpha_m}{1+(p(t-\tau)/p_h)^2}, \\ \dot{p}(t) &= -\gamma_p p(t) + \alpha_p \hat{m}(t),\end{aligned} \tag{B.12}$$

which is the same as (4.16).

Finally assuming that the mRNA dynamics are fast and replacing $\hat{m}(t)$ in the second equation in (B.12) with its steady-state value we arrive at

$$\dot{p}(t) = -\gamma_p p(t) + \frac{\kappa}{1+(p(t-\tau)/p_h)^2}, \tag{B.13}$$

where $\kappa = \alpha_m \alpha_p / \gamma_m$ that is the same as (4.6).

We remark that one may also obtain (B.13) by neglecting the mRNA dynamics in (B.1) and following the steps above yielding

$$\dot{p}(t) = -\gamma_p p(t) + \int_0^\infty w_e(\sigma) \frac{\kappa}{1+(p(t-\sigma)/p_h)^2} d\sigma \tag{B.14}$$

for the mean protein dynamics.

Author Manuscript Author Manuscript Author Manuscript Author Manuscript

References

1. Anderson RFV. The relative variance criterion for stability of delay systems. Journal of Dynamics and Differential Equations. 1993; 5(1):105–128.
2. Arkin A, Ross J, McAdams HH. Stochastic kinetic analysis of developmental pathway bifurcation in Phage λ-infected Escherichia coli cells. Genetics. 1998; 149(4):1633–1648. [PubMed: 9691025]
3. Arnold L, Crauel H, Wihstutz V. Stabilization of linear systems by noise. SI AM Journal on Control and Optimization. 1983; 21(3):451–461.
4. Basak GK. Stabilization of dynamical systems by adding a colored noise. IEEE Transactions on Automatic Control. 2001; 46(7):1107–1111.
5. Cloosterman MBG, van de Wouw N, Heemels WPMH, Nijmeijer H. Stability of networked control systems with uncertain time-varying delays. IEEE Transactions on Automatic Control. 2009; 54(7): 1575–1580.
6. Del Vecchio, D., Murray, RM. Biomolecular Feedback Systems. Princeton University Press; 2014.
7. Diekmann, O., van Gils, SA., Verduyn Lunel, SM., Walther, HO. Delay Equations: Functional-, Complex-, and Nonlinear Analysis, volume 110 of Applied Mathematical Sciences. Springer; 1995.
8. Engelborghs K, Luzyanina T, Roose D. Numerical bifurcation analysis of delay differential equations using dde-biftool. ACM Transactions on Mathematical Software. 2002; 28(1):1–21.
9. Erneux, T. Applied Delay Differential Equations, volume 3 of Surveys and Tutorials in the Applied Mathematical Sciences. Springer; 2009.
10. Farkas M, Stépán G. On perturbation of the kernel in infinite delay systems. Zeitschrift fur Angewandte Mathematik und Mechanik. 1992; 72(2):153–156.
11. Feldman, RM., Flores, CV. Applied Probability and Stochastic Processes. Springer; 2010.
12. Gao H, Chen T. New results on stability of discrete-time systems with time-varying state delay. IEEE Transactions on Automatic Control. 2007; 52(2):328–334.
13. Ghasemi, M., Zhao, S., Insperger, T., Kalmár-Nagy, T. Act-and-wait control of discrete systems with random delays; Proceedings of the American Control Conference; 2012. p. 5440-5443.
14. Gillespie DT. Exact stochastic simulation of coupled chemical reactions. The Journal of Physical Chemistry. 1977; 81:2340–2361.
15. Gupta C, López JM, Azencott R, Bennett MR, Josić K, Ott W. Modeling delay in genetic networks: From delay birth-death processes to delay stochastic differential equations. The Journal of Chemical Physics. 2014; 140(20):204108. [PubMed: 24880267]
16. Hartung F, Insperger T, Stépán G, Turi J. Approximate stability charts for milling processes using semi-discretization. Applied Mathematics and Computation. 2006; 174(1):51–73.
17. Insperger T, Stépán G. Semi-discretization method for delayed systems. International Journal for Numerical Methods in Engineering. 2002; 55(5):503518.
18. Insperger T, Stépán G. Stability analysis of turning with periodic spindle speed modulation via semidiscretization. Journal of Vibration and Control. 2004; 10(12):1835–1855.
19. Insperger, T., Stépán, G. Semi-discretization for Time-delay Systems: Stability and Engineering Applications, volume 178 of Applied Mathematical Sciences. Springer; 2011.
20. Insperger T, Stépán G, Turi. State-dependent delay in regenerative turning processes. Nonlinear Dynamics. 2007; 47(1-3):275–283.
21. Josić K, López JM, Ott W, Shiau L, Bennett MR. Stochastic delay accelerates signaling in gene networks. PLoS Computational Biology. 2011; 7(11):e1002264. [PubMed: 22102802]
22. Kats I. On the stability of systems with random delay in the first approximation. Prikladnaya Matematika i Mekhanika (P M M), translated as Journal of Applied Mathematics and Mechanics. 1967; 31(3):447–452.
23. Klumpp S. A superresolution census of RNA polymerase. Biophysical Journal. 2013; 105(12): 2613–2614. [PubMed: 24359730]
24. Kolmanovskii, VB., Nosov, VR. Stability of Functional Differential Equations, volume 180 of Mathematics in Science and Engineering. Academic Press Inc; 1986.

Author Manuscript Author Manuscript Author Manuscript Author Manuscript

25. Kolmanovsky, I., Maizenberg, TL. Stochastic stability of a class of nonlinear systems with randomly varying time-delay; Proceedings of the American Control Conference; 2000. p. 4304-4308.
26. Kushner, HJ. Introduction to Stochastic Control. Holt, Rinehart and Winston; 1971.
27. Kwiecińska AA. Stabilization of partial differential equations by noise. Stochastic Processes and their Applications. 1999; 79(2):179–184.
28. Lewis J. Autoinhibition with transcriptional delay: a simple mechanism for the zebrafish somitogenesis oscillator. Current Biology. 2003; 13(16):1398–1408. [PubMed: 12932323]
29. Lidskii EA. On stability of motion of a system with random delays. Differentialnye Uravnenia, translated as Differential Equations. 1965; 1(1):96–101.
30. Liu X, Shen J. Stability Theory of Hybrid Dynamical Systems With Time Delay. IEEE Transactions on Automatic Control. 2006; 51(4):620–625.
31. Longo DM, Selimkhanov J, Kearns JD, Hasty J, Hoffmann A, Tsimring LS. Dual delayed feedback provides sensitivity and robustness to the nf-κb signaling module. PLoS Computational Biology. 2013; 9(6)
32. Mackey MC, Longtin A, Lasota A. Noise-induced global asymptotic stability. Journal of Statistical Physics. 1990; 60(5-6):735–751.
33. Mallet-Paret J, Smith HL. The Poincaré-Bendixson theorem for monotone cyclic feedback systems. Journal of Dynamics and Differential Equations. 1990; 2(4)
34. Mao X. Exponential stability of stochastic delay interval systems with Markovian switching. IEEE Transactions on Automatic Control. 2002; 47(10):1604–1612.
35. Mather W, Bennett MR, Hasty J, Tsimring LS. Delay-induced degrade-and-fire oscillations in small genetic circuits. Physical Review Letters. 2009; 102(6):068105. [PubMed: 19257639]
36. McAdams HH, Arkin A. It's a noisy business! genetic regulation at the nanomolar scale. Trends in Genetics. 1999; 15(2):65–69. [PubMed: 10098409]
37. Michiels W, Van Assche V, Niculescu SI. Stabilization of time-delay systems with a controlled time-varying delay. IEEE Transactions on Automatic Control. 2005; 50(4):493–504.
38. Monk NA. Oscillatory expression of Hes1, p53, and NF-κb driven by transcriptional time delays. Current Biology. 2003; 13(16):1409–1413. [PubMed: 12932324]
39. Naganathan AN, Muñoz V. Scaling of folding times with protein size. Journal of the American Chemical Society. 2005; 127(2):480–481. [PubMed: 15643845]
40. Orosz G, Moehlis J, Murray RM. Controlling biological networks by time-delayed signals. Phil Trans of R Soc A. 2010; 368(1911):439–454. [PubMed: 20008410]
41. Park PG. A delay-dependent stability criterion for systems with uncertain time-invariant delays. IEEE Transactions on Automatic Control. 1999; 4(4):876–877.
42. Pu X, Zhao H. Stability of a kind of hybrid systems with time delay. Advances in Electronic Engineering, Communication and Management. 2012; 139:159–165.
43. Qin WB, Gomez MM, Orosz G. Stability and frequency response under stochastic communication delays with applications to connected cruise control design. IEEE Transactions on Intelligent Transportation Systems. 2015 submitted.
44. Roose, D., Szalai, R. Continuation and bifurcation analysis of delay differential equations. In: Krauskopf, B.Osinga, HM., Galan-Vioque, J., editors. Numerical Continuation Methods for Dynamical Systems, Understanding Complex Systems. Springer; 2007. p. 359-399.
45. Smith, H. An Introduction to Delay Differential Equations with Sciences Applications to the Life, volume 57 of Texts in Applied Mathematics. Springer; 2011.
46. Stépán, G. Retarded Dynamical Systems: Stability and Characteristic Functions, volume 210 of Pitman Research Notes in Mathematics. Longman; 1989.
47. Stricker J, Cookson S, Bennett MR, Mather WH, Tsimring LS, Hasty J. A fast, robust and tunable synthetic gene oscillator. Nature. 2008; 456:516–519. [PubMed: 18971928]
48. Tian T, Burrage K, Burrage PM, Carletti M. Stochastic delay differential equations for genetic regulatory networks. Journal of Computational and Applied Mathematics. 2007; 205(2):696–707.
49. Tigges M, Marquez-Lago TT, Stelling J, Fussenegger M. A tunable synthetic mammalian oscillator. Nature. 2009; 457:309–312. [PubMed: 19148099]

Author Manuscript Author Manuscript Author Manuscript Author Manuscript

50. Venturelli OS, El-Samad H, Murray RM. Synergistic dual positive feedback loops established by molecular sequestration generate robust bimodal response. Proceedings of the National Academy of Sciences of the United States of America. 2012; 109(48):E3324–33. [PubMed: 23150580]
51. Verriest EI, Michiels W. Stability analysis of systems with stochastically varying delays. Systems and Control Letters. 2009; 58(10-11):783–791.
52. Vogel U, Jensen KF. The RNA chain elongation rate in Escherichia coli depends on the growth rate. Journal of Bacteriology. 1994; 176(10):2807–2813. [PubMed: 7514589]
53. Xing-Cheng P, Wei Y. Stability of hybrid stochastic systems with time-delay. ISRN Mathematical Analysis. 2014 Article ID.
54. Yuan C, Mao X. Stability of stochastic delay hybrid systems with jumps. Eur J Control. 2010; 16:595–608.
55. Yue D, Zhang Y, Tian E, Peng C. Delay-distribution-dependent exponential stability criteria for discrete-time recurrent neural networks with stochastic delay. IEEE Transactions on Neural Networks. 2008; 19(7):1299–1306.

Author Manuscript Author Manuscript Author Manuscript Author Manuscript

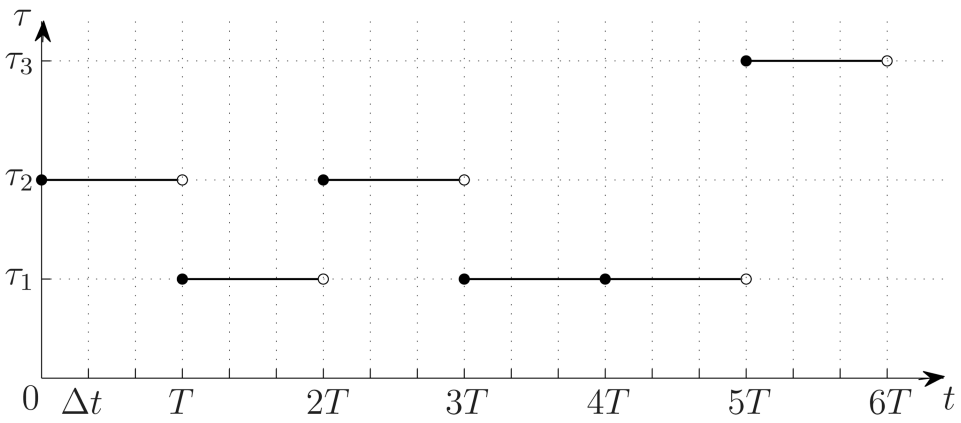

Figure 2.1.

A sample realization of the time evolution of the delay with $J = 3$ possible delay values. The delay remains constant for a holding time T while Δt denotes the discretization step.

Author Manuscript Author Manuscript Author Manuscript Author Manuscript

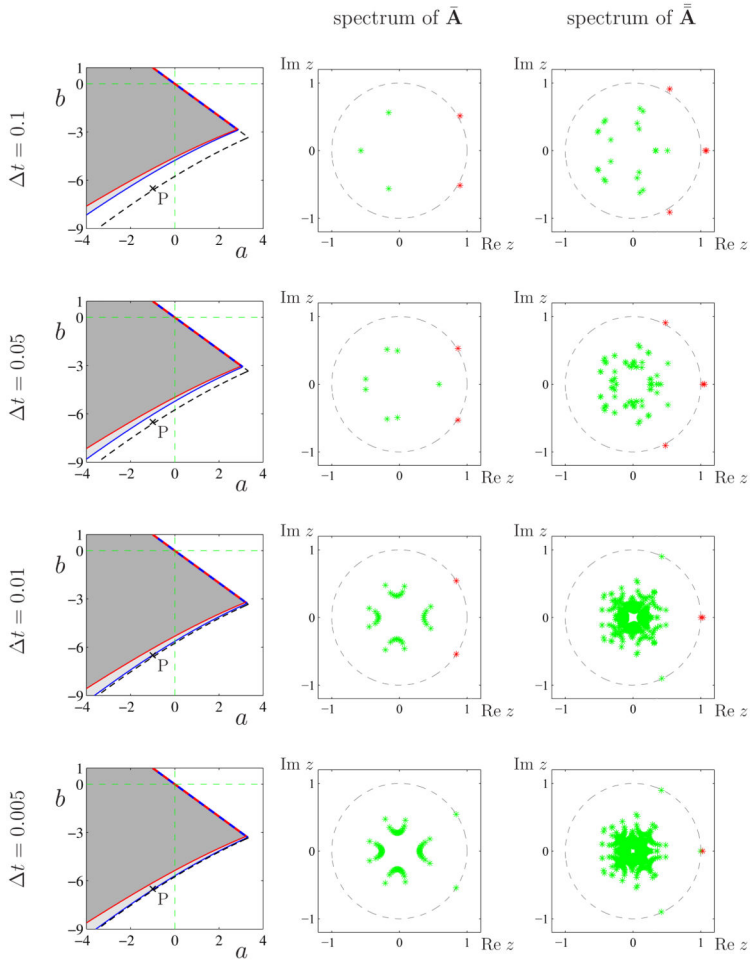

Figure 3.1.

Left column: Stability charts for system (3.11) with delay distribution $w(\sigma)=\frac{1}{3}\delta(\sigma-0.2)+\frac{1}{3}\delta(\sigma-0.3)+\frac{1}{3}\delta(\sigma-0.4)$ and the holding time $T = 0.1$ for different values of the discretization step Δt as indicated on the left. Blue curves are the stability boundaries for the mean while the red curves are the stability boundaries for the second moment. The dashed black curves are stability boundaries for the mean in the continuous limit. Light gray shading indicates mean stability and dark gray shading indicates second moment stability. Middle column: Eigenvalues for the discretized mean dynamics (matrix $\bar{\mathbf{A}}$) corresponding to point P located at $(a, b) = (-1, -6.5)$. Right column: Eigenvalues for the second moment dynamics (matrix $\bar{\bar{\mathbf{A}}}$) at point P. Stable eigenvalues are plotted as green while unstable eigenvalues are plotted as red.

Author Manuscript Author Manuscript Author Manuscript Author Manuscript

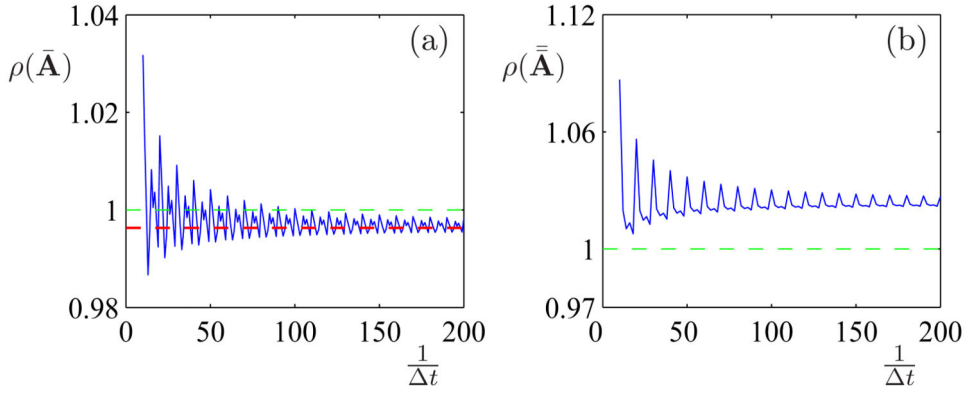

Figure 3.2.

The spectral radii of the matrices $\bar{\mathbf{A}}$ and $\bar{\bar{\mathbf{A}}}$ as functions of $1/\Delta t$ shown in panels (*a*) and (*b*), respectively. The horizontal dashed red line in (*a*) shows the value of $|e^{s_{1,2}T}|$ where $s_{1,2}$ are the leading characteristic roots of (3.15).

Author Manuscript Author Manuscript Author Manuscript Author Manuscript

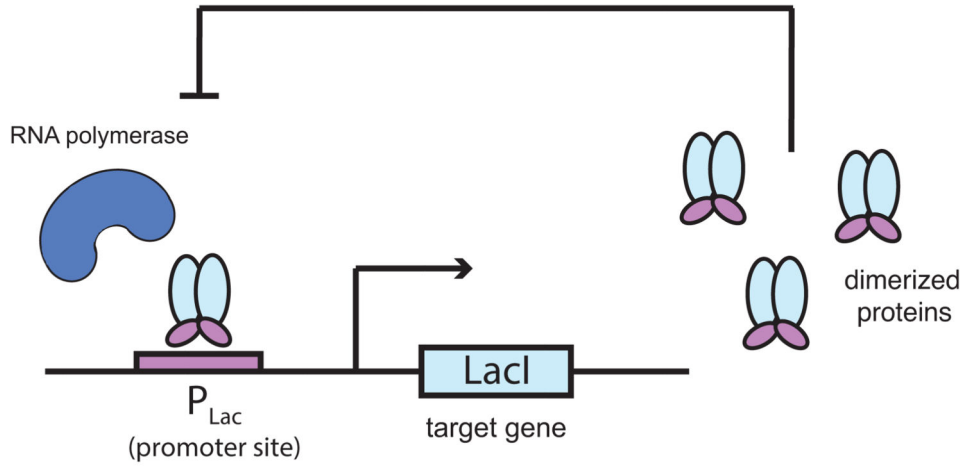

Figure 4.1.
An auto-regulatory gene network. The target gene codes for the protein LacI that represses its own production by blocking the RNA polymerase from binding.

Author Manuscript Author Manuscript Author Manuscript Author Manuscript

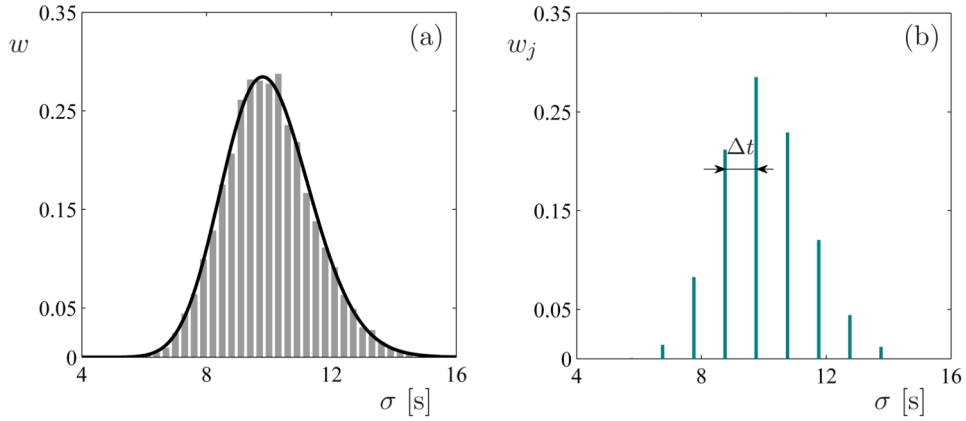

Figure 4.2.

(*a*) A normalized histogram of the delay obtained with running a Gillespie simulation for system (4.1) with $N = 50$ reactions and $c = 5$ reactions per second using the initial condition $P_0 = 10000$, $P_i = 0$, for $i = 1,\ldots, N$. The black curve shows the Erlang distribution (4.2) for the same parameters with mean $E = N/c = 10$ [s] and variance $V = N/c^2 = 2[\text{s}^2]$. (b) Discretization of the Erlang distribution using Dirac deltas separated by $\Delta t = 1$ [s].

Author Manuscript Author Manuscript Author Manuscript Author Manuscript

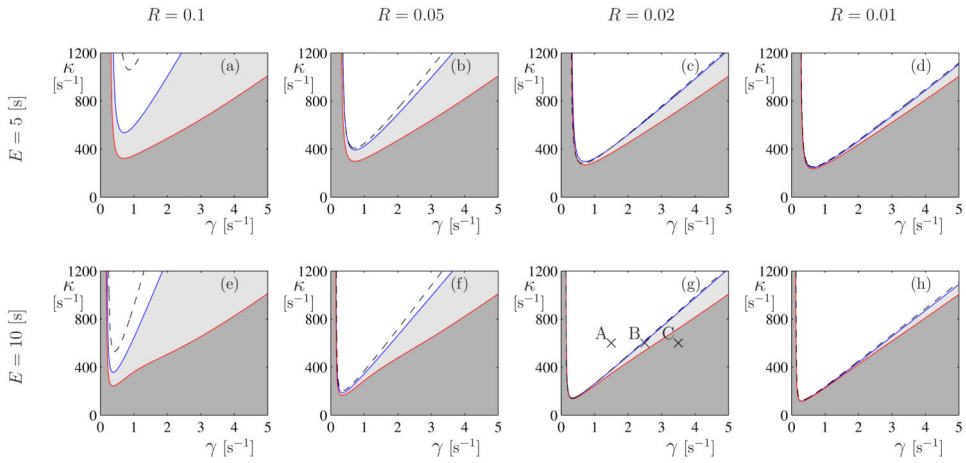

Figure 4.3.

Stability charts for system (4.8),(4.9) when the delay follows the Erlang distribution (4.2) for different values of the mean delay $E = N/c$ and relative variance $R = 1/N$. The holding time is set to $T = 1$ [s] and $\Delta t = 1$ [s]. The same notation is used as in the left column of Fig. 3.1.

Author Manuscript Author Manuscript Author Manuscript Author Manuscript

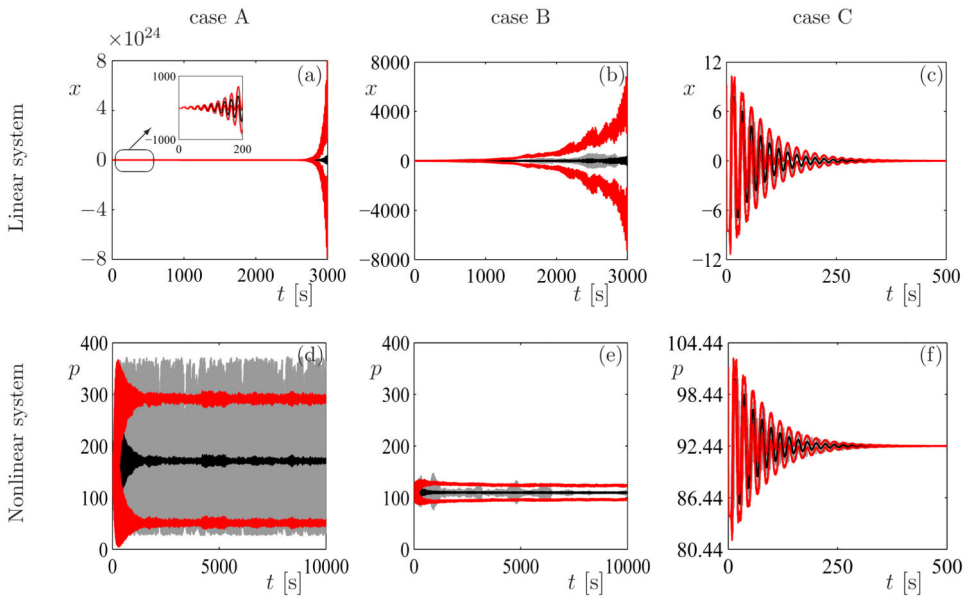

Figure 4.4.

(*a*–*c*) Numerical simulations of the linear model (4.8), (4.9) for points $A(\gamma, \kappa) = (1.5, 600)$, $B(\gamma, \kappa) = (2.5, 600)$, and $C(\gamma, \kappa) = (3.5, 600)$ marked in Fig. 4.3(g). (*d*–*f*) Corresponding simulation results of the nonlinear model (4.6). In each panel (*a*–*f*), the black trajectory indicates the mean while the red trajectories enclose mean ± standard deviation for 1000 runs and the gray curve shows a sample realization.

Author Manuscript Author Manuscript Author Manuscript Author Manuscript

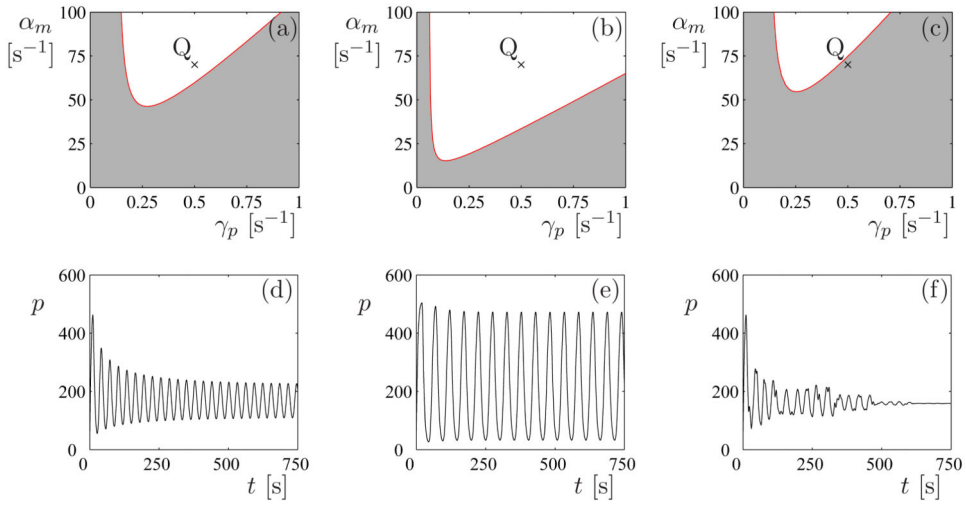

Figure 4.5.

Top panels: stability boundaries for the linearized system (2.2,4.19) with $\tau_1 = 10$ [s] and $\tau_2 = 20$ [s] and probability distribution $w_1 = u$, $w_2 = 1 - u$ for (*a*) $u = 1$, (*b*) $u = 0$, and (*c*) $u = 0.75$. Bottom panels: simulation results of the nonlinear model (4.16) for parameter values associated with point Q: $(\gamma_p, \alpha_m) = (0.5, 70)$. A sample trajectory of proteins as a function of time for (*d*) $u = 1$, (*e*) $u = 0$, and (*f*) $u = 0.75$. Note that panels (*d*) and (*e*) correspond to the deterministic systems with the single delay $\tau = 10$ [s] and $\tau = 20$ [s], respectively.

Author Manuscript Author Manuscript Author Manuscript Author Manuscript

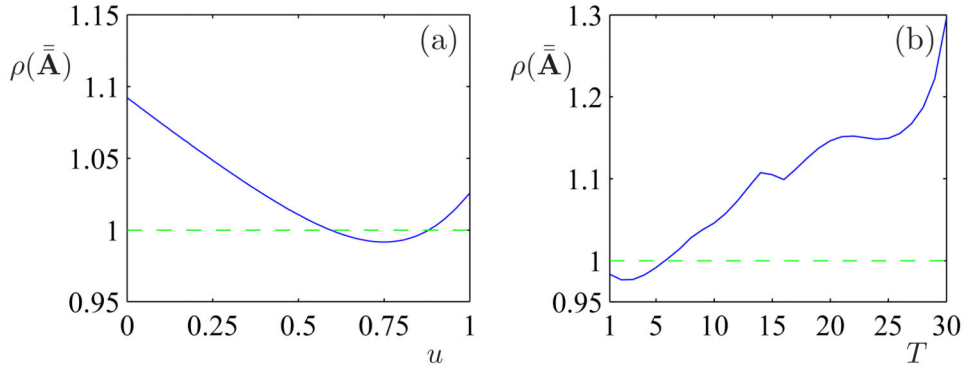

Figure 4.6.

(*a*) The spectral radius of $\bar{\bar{\mathbf{A}}}$ versus the probability distribution u. (*b*) The spectral radius of $\bar{\bar{\mathbf{A}}}$ versus the holding time T.